



Published in final edited form as:

Cell Rep. 2021 July 13; 36(2): 109372. doi:10.1016/j.celrep.2021.109372.

Inhibition of Rag GTPase signaling in mice suppresses B cell responses and lymphomagenesis with minimal detrimental trade-offs

Ana Ortega-Molina^{1,*}, Cristina Lebrero-Fernández¹, Alba Sanz¹, Nerea Deleyto-Seldas¹, Ana Belén Plata-Gómez¹, Camino Menéndez¹, Osvaldo Graña-Castro², Eduardo Caleiras³, Alejo Efeyan^{1,4,*}

¹Metabolism and Cell Signaling Laboratory, Spanish National Cancer Research Centre (CNIO), Melchor Fernandez Almagro 3, Madrid 28029, Spain

²Bioinformatics Unit, Spanish National Cancer Research Centre (CNIO), Madrid, Spain

³Histopathology Unit, Spanish National Cancer Research Centre (CNIO), Madrid, Spain

⁴Lead contact

SUMMARY

B lymphocytes are exquisitely sensitive to fluctuations in nutrient signaling by the Rag GTPases, and 15% of follicular lymphomas (FLs) harbor activating mutations in *RRAGC*. Hence, a potential therapeutic approach against malignant B cells is to inhibit Rag GTPase signaling, but because such inhibitors are still to be developed, efficacy and safety remain unknown. We generated knockin mice expressing a hypomorphic variant of RagC (Q119L); *RagC*^{Q119L/+} mice are viable and show attenuated nutrient signaling. B lymphocyte activation is cell-intrinsically impaired in *RagC*^{Q119L/+} mice, which also show significant suppression of genetically induced lymphomagenesis and autoimmunity. Surprisingly, no overt systemic trade-offs or phenotypic alterations caused by partial suppression of nutrient signaling are seen in other organs, and *RagC*^{Q119L/+} mice show normal longevity and normal age-dependent health decline. These results support the efficacy and safety of moderate inhibition of nutrient signaling against pathological B cells.

Graphical abstract

This is an open access article under the CC BY-NC-ND license (<http://creativecommons.org/licenses/by-nc-nd/4.0/>).

*Correspondence: aortegam@cnio.es (A.O.-M.), aefeyan@cnio.es (A.E.).

AUTHOR CONTRIBUTIONS

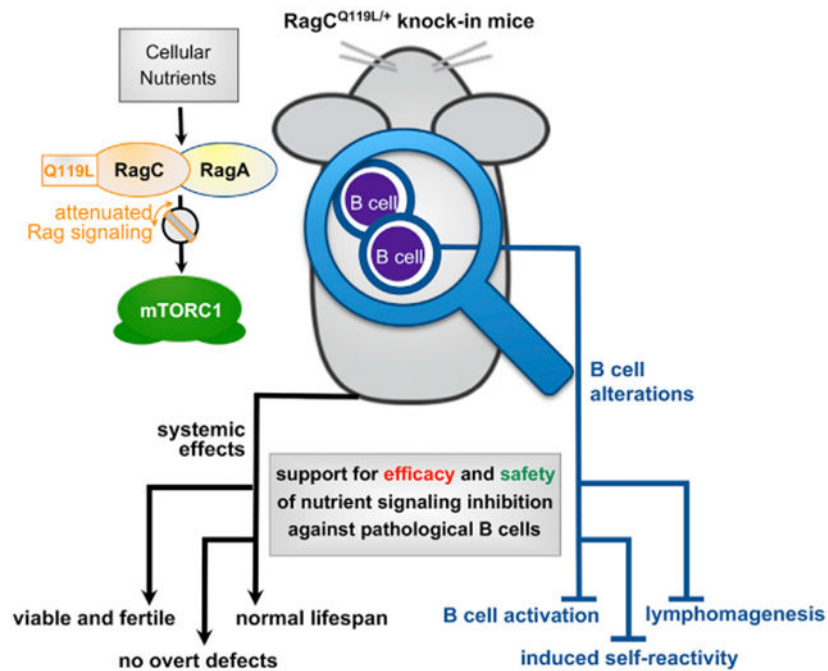
A.O.-M. performed most experiments; contributed to experimental design, data analysis, and manuscript writing; and secured funding. C.L.-F., A.S., N.D.-S., A.B.P.-G., and C.M. provided help with experimentation. O.G.-C. performed bioinformatics analysis of RNA-seq. E.C. performed and diagnosed histology and pathology. A.E. conceived and supervised the study, analyzed the data, wrote the manuscript, and secured funding. All authors read and commented on the manuscript and figures.

SUPPLEMENTAL INFORMATION

Supplemental information can be found online at <https://doi.org/10.1016/j.celrep.2021.109372>.

DECLARATION OF INTERESTS

The authors declare no competing interests.



In brief

By generating knockin mice expressing a hypomorphic variant of the RagC GTPase, Ortega-Molina et al. show that partial inhibition of nutrient signaling may be a safe and efficacious approach against pathogenic B cells and B cell lymphomas.

INTRODUCTION

Activation of B lymphocytes during the humoral response elicits a sudden proliferation with multiple rounds of division (Mesin et al., 2016; Victora and Nussenzweig, 2012). Such bursts are energetically onerous, and the master regulator of anabolism, mechanistic target of rapamycin complex 1 (mTORC1), is activated immediately after B cell activation, enabling cellular biomass accumulation before proliferation (Ersching et al., 2017). mTORC1 integrates inputs from growth factors and cytokines via the phosphatidylinositol 3-kinase (PI3K)-Akt signaling pathway and from cellular nutrient sufficiency via the Rag family of GTPases (Saxton et al., 2016; Shimobayashi and Hall, 2014; Valvezan and Manning, 2019). We have shown previously that B cells are particularly sensitive to dynamic control of nutrient signaling during activation, presumably because adequate sensing of nutrient sufficiency is key to ensure accomplishment of these onerous rounds of proliferation (Ersching et al., 2017). The exquisite effect and relevance of nutrient signaling for B cells is best exemplified by the exclusivity of nutrient signaling mutations in B cell lymphomas, particularly in follicular lymphoma (FL) (Green et al., 2015; Okosun et al., 2016; Ying et al., 2016).

FL is the second most frequent form of non-Hodgkin's lymphoma and remains incurable (Kahl and Yang, 2016; Matasar et al., 2019). FL cells derive from B cells that have participated in a transient anatomical structure involved in the humoral response, known

as the germinal center (GC) reaction, which enables production of high-affinity antibodies by iterative rounds of a two-step process consisting of affinity-based selective activation of antibody-producing B cells, followed by proliferation and antibody diversification (Bannard and Cyster, 2017; Mesin et al., 2016; Shlomchik and Weisel, 2012; Tas et al., 2016). Most FLs harbor a reciprocal translocation that juxtaposes the gene encoding the anti-apoptotic protein Bcl2 under the regulatory sequences of *IGH*, and additional genetic lesions include recurrent mutations in epigenetic modulators, in genes involved in interaction with the microenvironment (Huet et al., 2018; Matasar et al., 2019), and in genes responsible for signaling of cellular nutrient sufficiency to mTORC1 (Green et al., 2015; Kridel et al., 2016; Okosun et al., 2016; Ying et al., 2016). Mutations in nutrient signaling components upstream of mTORC1 occur in approximately 15% of individuals with FL and most frequently consist of point activating mutations in *RRAGC*, encoding the RagC GTPase. Rag GTPases exist in the cell as obligate heterodimeric complexes composed of RagA (or RagB) and RagC (or RagD), and in the presence of plentiful nutrient levels, RagA undergoes guanosine triphosphate (GTP) loading, and RagC loads guanosine diphosphate (GDP). This nucleotide configuration allows binding and recruitment of mTORC1 to the outer lysosomal surface, an essential step for kinase activation.

Ever since identification of the Rag GTPase pathway, there has been a relentless interest in potential therapeutic targeting of nutrient signaling as a strategy to selectively control mTORC1 activity (Chung et al., 2019; Kang et al., 2019; Sengupta et al., 2019). However, several questions regarding therapeutic targeting of nutrient signaling remain unanswered. (1) What would be a suitable indication for use of nutrient signaling inhibitors? (2) What extent of nutrient signaling inhibition would be efficacious and safe? In this regard, genetic elimination of Rag GTPase complexes is incompatible with embryonic development (Efeyan et al., 2014; Kim et al., 2014), and acute deletion causes rapid loss of the B cell lineage and also affects rapidly proliferative epithelial cells. But small-molecule-mediated targeting would result in partial inhibition, in contrast to acute genetic deletion. Whether a milder inhibition of nutrient signaling would result in effective versus on-target toxic and in what cell type or organ has not yet been determined.

We generated mice endogenously expressing a mutant variant of RagC (RagC^{Q119L}) that signals low levels of nutrients to mTORC1. Endogenous, heterozygous expression of RagC^{Q119L} shows a modest inhibitory effect in mTORC1 but impairs B cell activation upon immunization, GC formation, and plasma cell (PC) production. In the FL-prone background *VavP-Bcl2* (Egle et al., 2004), expression of *RagC*^{Q119L} suppresses lymphomagenesis and autoreactivity. Although efficacious to restrain B cell lymphomagenesis, expression of RagC^{Q119L} appears to be innocuous because whole-body expression of the RagC^{Q119L} variant did not compromise survival; neither did it affect age-dependent health decline or the prevalence or severity of aging-related pathologies.

RESULTS

RagC^{Q119L/+} knockin mice show a mild reduction in mTORC1 activity

We used CRISPR-Cas9 genome engineering (Wang et al., 2013) to generate *Rragc* knockin mice with a point mutation in the *Rragc* gene encoding a hypomorphic RagC GTPase variant

locked in a GTP-like state ($RagC^{Q119L}$) (Sancak et al., 2008; Shen et al., 2017; Figure S1A). Homozygous $RagC^{Q119L/Q119L}$ mice were never found by breeding heterozygous progenitors (Figure S1B and S1C), consistent with the *in utero* lethality observed in mice with genetic loss of the Rag GTPase complex (Efeyan et al., 2014; Kim et al., 2014). Heterozygous $RagC^{Q119L/+}$ mice were obtained at Mendelian ratios (Figure S1D), were macroscopically normal, and showed no overt differences in body weight or in organ weight after sacrifice (Figure 1A).

To assess potential consequences of the expression of this mutation in bone marrow (BM)-derived cells, we quantified the proportions of mature populations of the hematopoietic lineage in the blood and spleen. Lymphoid and myeloid populations were present in $RagC^{Q119L/+}$ mice at frequencies similar to those of wild-type counterparts in the blood (Figure S1E) and spleen (Figure 1B; Figure S1F). In addition, similar numbers of stem cells and lymphoid and myeloid progenitors were found in BM from $RagC^{+/+}$ and $RagC^{Q119L/+}$ mice (Figure S1G). Together with analysis of subpopulations of splenic B cells (marginal zone, transitional, and follicular B cells; Figure S1H), these data show that heterozygous expression of $RagC^{Q119L/+}$ has no effect on maturation of BM-derived cells.

We next assessed the effect of endogenous expression of $RagC^{Q119L}$ on nutrient-mediated regulation of the mTORC1 pathway in mouse embryonic fibroblasts (MEFs). Amino acid starvation followed by acute stimulation with amino acids at different times (Figure 1C; quantification in Figure S1I) resulted in a minimal but evident decrease in phosphorylation of the canonical mTORC1 target S6K1 in $RagC^{Q119L/+}$ MEFs compared with $RagC^{+/+}$ cells. A modest impairment of activation of mTORC1 in $RagC^{Q119L/+}$ cells is also seen as a decreased fraction of the up-shifted (phosphorylated) band of Transcription Factor EB (TFEB), another target of mTORC1, upon re-stimulation (Figure 1C; Figure S1I). Similarly, primary hepatocytes derived from $RagC^{Q119L/+}$ mice showed a similar mild but consistent decrease in mTORC1 activity (Figure 1D; Figure S1J).

We next determined mTORC1 activity in different subpopulations of B cells (naive, GC B cells, and PCs) *in vivo* from $RagC^{+/+}$ and $RagC^{Q119L/+}$ mice immunized with sheep red blood cells (SRBCs). mTORC1 activity was reduced significantly in naive B cells, GC B cells, and PCs (Figure 1E; Figures S1K and S1L) from $RagC^{Q119L/+}$ mice, as revealed by intracellular staining of S235/236-phospho-S6. RNA sequencing of GC B cells from immunized $RagC^{+/+}$ and $RagC^{Q119L/+}$ mice showed minimal differences in gene expression (Table S1), which included signatures associated with reduced mTORC1 activity *in RagC^{Q119L/+}* mice, such as reduced translation and ribosome signatures, a reduction in *c-myc* target genes, depletion of genes upregulated in $RRAGC^{mut}$ individuals with FL, and enrichment of genes downregulated in $RagC^{S74C/+}$ GC B cells (Figure 1F; Figure S1M).

We conclude that suppression of mTORC1 signaling by heterozygous expression of $RagC^{Q119L}$ is innocuous or at least of minimal effect *in vivo* and causes a modest decrease in activation of mTORC1 by nutrients.

RagC^{Q119L/+} mice show a B-cell-intrinsic impaired humoral response *in vitro* and *in vivo*

We have determined previously that genetic activation of the Rag GTPase pathway has different effects in the humoral response, depending on the strength of signaling activation (Ersching et al., 2017; Ortega-Molina et al., 2019). Thus, the effect of heterozygous expression of the hypomorphic RagC^{Q119L} mutation could have on B cell functions was unpredictable. We induced GC formation in *RagC^{Q119L/+}* mice by intraperitoneal injection of SRBC, followed by analysis of several markers of the humoral response (Figure S2A). We observed a two-thirds reduction in GC cells and GC size *in vivo* (Figures 2A and 2B; Figures S2B and S2C) in *RagC^{Q119L/+}* mice, with normal GC B cell proliferation *in vivo* (Figure S2D) and a negligible effect on the GC dark zone/light zone ratio (Figure S2E). Such an impaired GC response correlated with decreased PC production (Figure 2C; Figure S2F), and also decreased was the abundance of class-switched immunoglobulin G₁ (IgG₁)⁺-producing *RagC^{Q119L/+}* PCs and total IgG₁⁺ GC B cells (Figure 2D; Figure S2G). As expected by the reduction in PC numbers, titers of IgM and IgG₁ antibodies were decreased in sera from immunized *RagC^{Q119L/+}* mice (Figures 2E and 2F). Marginal zone, transitional, and follicular B cell subpopulations remained unchanged in immunized *RagC^{Q119L/+}* mice (Figure S2H). Follicular helper T and follicular regulatory T cell numbers were normal in immunized *RagC^{Q119L/+}* mice (Figure S2I and S2J), suggesting that inhibition of nutrient signaling does not compromise B cell activation indirectly by affecting the GC T cell microenvironment. Consistently, *ex vivo* activation of isolated naive B cells with anti-CD40 and interleukin-4 (IL-4) replicated the impaired B cell activation observed *in vivo*: *RagC^{Q119L/+}* B cells showed reduced class-switch recombination (CSR) (Figure 2G; Figure S2K) and reduced cell proliferation *in vitro*, measured by decay of Carboxyfluorescein succinimidyl ester (CFSE) (Figure 2H; Figure S2L). In contrast, *in vitro* stimulation of T cells with anti-CD3 and anti-CD28 yielded identical percentages of activated T cells (Figures S2M and S2N).

To provide additional support for the cell-intrinsic inability of *RagC^{Q119L/+}* B cells to unleash a humoral response and to assess whether *RagC^{Q119L/+}* B cells have a competitive disadvantage compared with *RagC^{+/+}*, we performed competitive reconstitution of lethally irradiated hosts by co-injection of CD45.1/.2 *RagC^{+/+}* mixed with *RagC^{+/+}* or *RagC^{Q119L/+}* CD45.2/.2 BM cells at a 1:1 ratio (Figure S2O). Eight weeks after reconstitution, we monitored the relative abundance of CD45.2/.2 *RagC^{+/+}* and *RagC^{Q119L/+}* naive B cells, which was at a 45:55 proportion with the competing CD45.1/.2 *RagC^{+/+}* cells, mildly but significantly different from the expected 50:50 proportion when assuming neutral competitiveness (Figure S2P). The *RagC^{Q119L/+}* monocytic population was also reduced in this competitive setting, whereas CD4⁺ and CD8⁺ T cells, neutrophils, and eosinophils showed a 1:1 ratio. Ten days after immunization with SRBCs, the relative abundance of *RagC^{Q119L/+}* GC B cells and PCs dropped to 20:80, whereas the T follicular helper (Tfh) cell population remained unaffected (Figure 2I). This result demonstrates the intrinsic inability of *RagC^{Q119L/+}* B cells to become activated, with normal responses of the *RagC^{+/+}* B cells coinhabiting the same immunized wild-type host. Importantly, the reduction in PC and GC *RagC^{Q119L/+}* populations occurred with decreased mTORC1 activity (Figure 2J). The *in vitro* activation and *in vivo* competition experiments show that heterozygous

expression of RagC^{Q119L} is inconsequential for B cell lineage development but confers on RagC^{Q119L/+} B cells a cell-intrinsic inability to become activated upon immunization.

To further confirm the B-cell-intrinsic nature of the decreased humoral response by expression of RagC^{Q119L}, we undertook another genetic approach consisting of BM reconstitution of irradiated hosts with 90% *Ighm*^{μMT/μMT} hematopoietic stem cells (HSCs), which are unable to produce a B cell lineage (Kitamura et al., 1991), plus 10% of RagC^{+/+} or RagC^{Q119L/+} HSCs (Figure S2Q). With this approach, non-B cell populations derive almost exclusively from *Ighm*^{μMT/μMT} HSCs, whereas the B cell lineage is contributed entirely by RagC^{Q119L/+} progenitors (or RagC^{+/+}, in control mice). When immunized with SRBCs, we observed that restricted expression of RagC^{Q119L/+} to B cells sufficed to impair GC development (Figure 2K) and PC production (Figure 2L), mirroring the impairment seen in RagC^{Q119L/+} mice. The *in vitro* and *in vivo* experiments show that the compromised humoral response in RagC^{Q119L/+} mice is B cell intrinsic.

RagC^{Q119L/+} mice exhibit delayed follicular lymphomagenesis

We next sought to determine whether moderate suppression of nutrient signaling could also suppress the oncogenicity caused by expression of VavP-Bcl2 (Egle et al., 2004). Indeed, FL and high-grade lymphoma development was delayed significantly in *VavP-Bcl2*^{Tg}; RagC^{Q119L/+} mice (Figures 3A-3C), which correlated with smaller spontaneous GC formation and reduced SRBC-induced GC populations in young mice (Figures 3D and 3E; Figures S3A-S3C) and reduced incidence of FL measured at 250 days (Figure 3F). All tumors showed pathognomonic features of FL (Figure S3D) and a similar Ki67 proliferative index (Figure S3E).

Although with delayed manifestation, the incidence and grade of FL at euthanasia were unaffected by endogenous heterozygous expression of the RagC^{Q119L} variant in the presence of *VavP-Bcl2*^{Tg} (Figure 3G), and so were the tumor burden (Figure S3F) and PD1⁺ microenvironment (Figure S3G), compared with *VavP-Bcl2*^{Tg}; RagC^{+/+} mice.

Importantly, not only was FL delayed by expression of the Q119L mutation but also the concomitant development of autoimmune disease (Figures 3H and 3I; Figure S3H), so both pathological outcomes of B cells expressing the Bcl2 transgene are partially prevented by mild impairment of nutrient signaling.

RNA sequencing analysis of sorted FL cells from *VavP-Bcl2*^{Tg}; RagC^{+/+} and *VavP-Bcl2*^{Tg}; RagC^{Q119L/+} tumor-bearing mice revealed changes in *VavP-Bcl2*^{Tg}; RagC^{Q119L/+} samples of reduced mTORC1 activity, increased expression levels of TFEB targets, and depletion of genes upregulated in GCs and FLs from mice expressing the RagC mutant variants T89N and S74C, plus a reduction in glycolysis and robust signatures of suppressed activity of the oncogenic pathways nuclear factor κB (NF-κB) and Janus kinase (JAK)-signal transducer and activator of transcription (STAT) pathway (JAK-STAT) (Table S2; Figure 3J; Figures S3I-S3M).

These results show that moderate genetic inhibition of nutrient signaling suppresses pathological B cell activation and lymphomagenesis and suggest that mild inhibition

of nutrient signaling achieved by restricting intake or with a pharmacological inhibitor targeting the nutrient signaling pathway could be efficacious to delay FL development and to restrain autoreactivity.

***RagC*^{Q119L/+} mice have a normal lifespan**

The delayed lymphomagenesis in *VavP-Bcl2*^{Tg}; *RagC*^{Q119L/+} mice suggests that even mild inhibition of the nutrient signaling pathway could be conceived as an intervention against aberrant B cell function, but its long-term effect or pleiotropic negative trade-off in other cells and organs could limit potential therapeutic benefits. Hence, to search for potential negative effects related to mild and chronic inhibition of nutrient signaling that may not manifest obviously early on but could affect health or survival later in life, we aged colonies of *RagC*^{+/+} and *RagC*^{Q119L/+} mice and determined their longevity, the probable cause of death, prevalence of common pathologies, and any unexpected phenotypic alterations. *RagC*^{Q119L/+} mice had a normal lifespan (Figure 4A; Figure S4A). Interestingly, the mean longevity of the oldest 20% of *RagC*^{Q119L/+} females was increased significantly (+9%, $p = 0.035$) (Figure S4A). Exhaustive anatomopathological examination of aged cohorts of *RagC*^{+/+} and *RagC*^{Q119L/+} mice revealed no differences in malignant tumor incidence or severity at euthanasia (Figure 4B). Excluding all mice that developed cancer, the longevity of *RagC*^{Q119L/+} mice was equal to that of *RagC*^{+/+} mice (Figure 4C). Furthermore, we measured well-known aging-related features and parameters of health decline in old *RagC*^{Q119L/+} mice (Bellantuono et al., 2020). *RagC*^{Q119L/+} mice presented equivalent increases in body weight during aging (Figure S4B) and similar glucose levels at old age compared with aged-matched *RagC*^{+/+} mice (Figure S4C), a similar decline in neuromuscular coordination as measured by tightrope assay and rotarod test (Figures 4D and 4E), and similar dermal skin thickness (Figure 4F). No changes in peripheral blood composition or differences in inflammatory cells in the spleen, with the exception of a small decrease in dendritic cells (DCs), were observed in old *RagC*^{Q119L/+} versus old *RagC*^{+/+} mice (Figure 4G; Figures S4D and S4E). *RagC*^{Q119L/+} 500-day-old males showed a slight increase in bone mineral density compared with old *RagC*^{+/+} mice (Figure 4H). Surrogate biochemical parameters of liver damage revealed no differences between genotypes at old age (Figure S4F) or differences in BM stem cell populations (Figure S4G). Finally, markers of age-associated senescence and a senescence-associated secretory phenotype (SASP) in kidneys from old *RagC*^{Q119L/+} and *RagC*^{+/+} mice were similar (Figures 4I and 4J). Thus, the multiparameter analysis of aged cohorts of *RagC*^{Q119L/+} mice revealed no effects of mild systemic chronic reduction of Rag GTPase signaling on longevity and age-related pathologies.

The strong suppressive effects on pathogenic B cells without obvious negative trade-off effects in *RagC*^{Q119L/+} mice strongly support the efficacy and safety of nutrient signaling inhibitors against B cell pathologies.

DISCUSSION

Our results show that mild suppression of nutrient signaling, driven by expression of a hypomorphic mutant variant of the RagC GTPase under endogenous regulation in mice,

has a significant suppressive effect on B cell activation and lymphomagenesis without compromising mouse physiology and longevity.

RagC^{Q119L/Q119L} mice are not viable, consistent with the failure of embryonic development seen in RagA knockout and RagA/B double knockout mice (Efeyan et al., 2014; Kim et al., 2014). In contrast, RagC^{Q119L/+} mice showed minimal phenotypic alterations. This work and several previous efforts by us and others have shown that alterations in nutrient signaling preferentially affect B cells with minimal consequences for other cell types and organs. Acute genetic elimination of the heterodimeric Rag GTPase complex selectively suppresses B cell maturation without mirrored negative effects on T cell maturation (Do et al., 2020; Efeyan et al., 2014; Kalaitzidis et al., 2017; Kim et al., 2014). Conversely, genetic activation of RagA, conferring complete insensitivity to nutrient deprivation (de la Calle Arregui et al., 2021; Efeyan et al., 2013), results in compromised B cell activation upon immunization (Ersching et al., 2017). Milder activation of Rag GTPases in mice by heterozygous expression of mutant variants of RagC found in human B cell lymphomas results in accelerated lymphomagenesis and hyperactive B cells (Ortega-Molina et al., 2019). Sequencing efforts have identified that activating mutations in Rag GTPases are detected exclusively in GC lymphomas (Green et al., 2015; Kridel et al., 2016; Okosun et al., 2016; Ying et al., 2016). Although speculative, an appealing explanation for this uniqueness resides in the fact that naive B cells are among the smallest cells in the body, with minimal cytoplasmic content and, hence, limited anabolic capacity. Activation of the humoral response demands a rapid proliferative burst of GC B cells (Mesin et al., 2016; Victora and Nussenzweig, 2012). Only when a B cell has the building blocks and energy required for enduring the onerous process of anabolism can it successfully accomplish the rapid proliferative burst. Thus, nutrient sensing is critical to ensure that the anabolic demand is met by cellular nutrients.

Although rapalogs and ATP-competitive inhibitors can block mTORC1, partial blockade of some targets of mTORC1 by rapalogs and the on-target toxicity of blocking mTORC1 and mTORC2 by ATP-competitive inhibitors of mTOR demand additional approaches to selectively target all functions of mTORC1 (Saxton and Sabatini, 2017; Zoncu et al., 2011). Moderate suppression of mTORC1 signaling by expression of this hypomorphic variant suggests that even moderate pharmacological inhibition of Rag GTPases may be efficacious to functionally and selectively block mTORC1 activity in activated B cells. Such moderate suppression may be well-tolerated by other cells and organs and be efficacious and safe. Although suppressive effects of the Q119L variant of RagC on FL are consistent with potential efficacy of nutrient signaling inhibitors in B cell lymphomas, no acute genetic inhibition of RagC was feasible with this genetic system, so a tumor-suppressive function of decreased RagC signaling may also be related to a decreased pool of activated B cells susceptible to transformation.

The mTOR signaling pathway plays a significant role in longevity by regulating several hallmarks of aging (López-Otín et al., 2013; Singh et al., 2019). Work in yeast, worms, and mice with pharmacologic and genetic inhibition of mTORC1 supports a beneficial effect on longevity (Saxton and Sabatini, 2017; Singh et al., 2019). Hence, therapeutic inhibition of mTORC1 signaling has gathered a lot of attention as a promising anti-aging intervention.

Moreover, one of the most efficient interventions against aging is restriction of dietary intake (dietary restriction, DR), and the beneficial effects of DR are thought to be, at least in part, due to inhibition of mTOR (Anderson et al., 2018; Gems and Partridge, 2013). Here we have shown that *RagC^{Q119L/+}* mice have normal longevity and similarly develop age-dependent health decline, according to several markers of aging (Bellantuono et al., 2020). We believe that these results do not contradict the notion of inhibition of mTORC1 to combat human aging. The effect of expression of *RagC^{Q119L}* in heterozygosity results in only mild inhibition of nutrient signaling, and it is conceivable that a certain threshold of inhibition of mTORC1 signaling must be reached to reveal its longevity-promoting effects, as seen genetically in mice expressing a mTOR hypomorph allele (Wu et al., 2013) or in *S6K1* homozygous knockout female mice (Selman et al., 2009). The life-extending effects of caloric restriction in C57BL/6 mice are only seen when the limitation exceeds 20% of the *ad-libitum*-ingested calories (Ingram and de Cabo, 2017; Liao et al., 2010; Mitchell et al., 2016). Hence, we postulate that mild inhibition of nutrient signaling has large consequences for active and pathological B cells, which are exquisitely sensitive, but may not reach the threshold of an inhibitory effect on mTORC1 for a systemic effect.

RagC^{Q119L/+} mice revealed that aberrant B cell activation and its pathological outcomes can be modulated by systemic moderate inhibition of nutrient signaling without prominent physiological trade-offs or undesired side effects.

STAR★METHODS

RESOURCE AVAILABILITY

Lead contact—Further information and requests for resources and reagents should be directed to and will be fulfilled by the Lead Contact, Alejo Efeyan (aefeyan@cniio.es).

Materials availability—Mouse lines generated in this study are available from the Lead Contact with a completed Materials Transfer Agreement.

Data and code availability—Sequence data that support the findings of this study have been deposited in GEO, with the accession codes GEO: GSE174004, GSE174003 and GSE173619. This work does not report original code. Any additional information required to reanalyze the data reported in this paper is available from the lead contact upon request.

EXPERIMENTAL MODEL AND SUBJECT DETAILS

All animal procedures carried out at the CNIO were performed according to protocols approved by the CNIO-ISCIII Ethics Committee for Research and Animal Welfare (CEIyBA). *Ighm^{μMT}* mice (Kitamura et al., 1991) were obtained from Jackson Laboratories (JAX stock #002288). *VavP-Bcl2* mice (Egle et al., 2004) were obtained from Suzanne Cory Lab. The age and gender of all experimental mice are stated in each figure legend. Unless otherwise stated in the figure legends, males and females were used for the same experiment. Mice were housed under specific pathogen-free (SPF) conditions, at 22°C, and with 12-hr dark/light cycles (light cycle from 8:00am to 8:00pm). Mice were fed with a standard chow diet (Harlan Teklad 2018). All mice were observed weekly by trained

personnel. Upon signs of morbidity, mice were closely inspected daily until application of *Humane End Point* (HEP) criteria (<https://www.nationalacademies.org/global/ilar/Guide>). From our experience, the humane end point is applied when the life expectancy of the mice is on average shorter than one week.

METHOD DETAILS

Generation of RagC Crispr-edited KI mice—To introduce the Q119L *RRAGC* mutation, mouse blastocysts were injected with the Cas9 mRNA, a single-guide RNA (sgRNA) targeting the sequence of interest (mouse *Rragc*), and a single-stranded DNA oligo (ssDNA) containing the desired mutation flanked by 40–60 bases homologous to the sequence adjoining the DNA double-strand break (DSB). Following clone selection, genotyping was performed by specific PCR followed by restriction fragment length polymorphisms (RFLP) or Sanger sequencing. For introducing the CAG to CTC mutation, translating into Q119L, we utilized a gRNA with the following sequence (in minus orientation): TCAAAGAAGTCCATCTGCCCCAGG. A repair oligo consisted of single-stranded DNA with the CTC mutation plus additional silent mutations within the sequence used for the gRNA: ACTCATGGATTTTTTTGA.

Mouse experimentation

Immunizations: For the generation of GC response, 8-10 week old mice were immunized by intraperitoneal (i.p.) injection of (1×10^9) Sheep Red Blood Cells (SRBC, *Oxoid*, #SR0053B) in PBS and analyzed at day 10. To measure proliferation in GC B cells, mice were immunized by intraperitoneal injection of (1×10^9) SRBC, and after 10d, 2 hours prior to sacrifice, mice were intraperitoneal injected with 0.5 mg of EdU. Analysis of EdU incorporation was performed using the Click-iT® Plus EdU Alexa Fluor® 647 Flow Cytometry Assay Kit (*Life Technologies*, #C10634) following manufacturer instructions.

Metabolic parameters: Blood was collected from the tail tip to determine glucose levels using Accu-check Aviva glucose strips. Blood was collected from the sub-mandibular vein to measure white blood count determined by a blood cell counter (CVM LaserCell) and to measure ALT, BUN and cholesterol using VetScan mammalian liver profile rotors (Abaxis, # 500-0040-12).

Behavioral tests—For the tightrope assay, mice were placed on a bar of circular section (60 cm long and 1.5 cm diameter) and the test was considered successful when a mouse stayed on the bar for 60 s in a least one trial out of 5 consecutive trials (Ortega-Molina et al., 2012). The rotarod test was used to evaluate motor coordination and balance in mice. Tests were performed in a rotarod apparatus (Panlab model LE 8200) using a continuous acceleration protocol from 4 to 40 rpm in a period of 120 s. Time to fall was recorded, and the average of three trials was used in the quantification (Whittemore et al., 2019).

Signaling in mouse embryonic fibroblasts—Sub-confluent cell cultures were rinsed three times and were placed in RPMI without amino acids, supplemented with 10% dialyzed FBS, during 45 minutes. Re-stimulation with amino acids was performed for the indicated times with the concentration of amino acids present in RPMI.

Signaling in primary hepatocytes—Primary hepatocytes were cultured at a confluence of 300000 cells per well in collagen-coated (*Sigma-Aldrich* #C3867) multi six-well plates. After 6 hours the media was changed, and hepatocytes were cultured overnight before any experimental procedure. The next day, cells were rinsed three times and placed in DMEM:F12 without amino acids (*USBiological Life Science* #D9807-10) supplemented with 6mM NaHCO₃ (*Sigma* #1063291000), 18mM HEPES pH 7.4 (*Lonza* #17-737E), 25 mM glucose (*Sigma-Aldrich* #G8769) and 10% dialyzed FBS during 1 hour. Re-stimulation with amino acids was performed for the indicated times.

Class-switch recombination *in vitro*—To study the process of class-switch recombination (CSR), we isolated CD43⁻ resting B cells from non-immunized mice using magnetic beads, (*Miltenyi Biotech* #130-049-801) following manufacturer instructions. Cells were washed and resuspended in B cell medium (RPMI (*Sigma* #R8758) +10% FBS (*Hyclone* #SV30160.03) +55 μM β-mercaptoethanol (*GIBCO*, #31350-010) +10mM HEPES (*Lonza* #BE17-737E) +100ug/mL penicillin/streptomycin (*GIBCO*, #15070-063) containing 1ug/mL anti-CD40, (*R&D Systems*, #MAB440) and 25ng/mL mouse Interleukin-4 (*R&D Systems*, #404-ML). The culture medium was replenished every two days to avoid exhaustion. Four days later, cells were harvested and processed for flow cytometry analysis.

B cell proliferation—To study cell proliferation in activated B cells, CD43⁻ resting B cells were labeled with 1.2 μM CFSE for 10 minutes (*Life Technologies* #C34554) following manufacturer instructions. This reagent monitors distinct generations of proliferating cells by a fluorescent dye dilution. Data were acquired at days 1 to 4 on a FACSCanto II (*BD Biosciences*) flow cytometer with 488nm excitation and an emission filter in the 530/30nm.

T cell activation and proliferation—To study T cell activation and proliferation, T cells were isolated from spleen of non-immunized mice using magnetic beads (*Miltenyi Biotech*, #130-104-454) following manufacturer instructions. To study T cell activation, 2x10⁶cells/ml of CD4⁺ T cells were seeded in an anti-CD3 (5 μg/ml; *Tonbo Biosciences* #40-0031) -coated plate and in the presence of anti-CD28 antibody (2 μg/ml; (*Tonbo Biosciences*, #40-0281) in culture medium (RPMI (*Sigma* #R8758) +10% FBS (*Hyclone* #SV30160.03) +55 μM β-mercaptoethanol (*GIBCO*, #31350-010) +10mM HEPES (*Lonza* #BE17-737E) +100 μg/mL penicillin/streptomycin (*GIBCO*, #15070-063)). To study cell proliferation in activated T cells, isolated CD4⁺ cells were labeled with 1.2 μM CFSE for 5 minutes (*Life Technologies*, #C34554) following manufacturer instructions. CD4⁺ T cells were analyzed at day 3 for activation and proliferation by flow cytometry.

Staining and flow cytometry analysis—Mononuclear cell pools were isolated from mouse spleens at the indicated times post-immunization. Cells were separated by crushing the spleens through a 70-micron mesh (*Corning*) in ice-cold PBS +0.1% BSA +3mM EDTA, and red blood cells were lysed using Erythrocyte Lysis Buffer (*QIAGEN*, #79217). Cell staining was performed on ice in PBS +0.1% BSA +3mM EDTA. We included a prior step of incubation with Fc-block Reagent (Anti-CD16/CD32, *BD Pharmigen*,

#553142). GC B cells were identified within the B cell fraction (B220⁺) as GL7⁺ CD95⁺. Alternatively, GC B cells were identified within the CD19⁺ cell fraction, as CD95⁺CD38⁻. Plasma cells were identified by gating on CD138⁺, B220^{lo} cells. T follicular helper cells (Tfh) were identified as B220⁻/CD4⁺/CXCR5⁺/PD-1⁺/Foxp3⁻ and T follicular regulatory cells (Tfr) were identified as B220⁻/CD4⁺/CXCR5⁺/PD-1⁺/Foxp3⁺. DZ GC B cells were identified as CD19⁺/CD95⁺/CD38⁻/CXCR4⁺CD86^{lo} while LZ GC B cells were identified as CD19⁺/CD95⁺/CD38⁻/CXCR4^{lo}CD86⁺. Follicular B cells were identified as Tcrb⁻/CD19⁺B220⁺/IgD^{hi}IgM^{lo}. Marginal zone and transitional type 1 (T1) B cells were identified (as one population) as Tcrb⁻/CD19⁺B220⁺/IgD^{lo}IgM^{hi}, according to Béguelin et al. (2013). Transitional type 2 (T2) B cells were identified as Tcrb⁻/CD19⁺B220⁺/IgD^{hi}IgM^{hi}. Macrophages were identified as F/480⁺SSC^{hi}. NK cells were identified as F/480⁻B220⁻/CD3⁻/NK.1.1⁺. Dendritic cells were identified as F/480⁻B220⁻/CD3⁻/NK.1.1⁻/MHCII⁺/CD11c⁺. Neutrophils were identified as F/480⁻B220⁻/CD3⁻/NK.1.1⁻/MHCII⁻/CD11c⁻CD11b⁺/Ly6G⁺. Monocytes were identified as F/480⁻B220⁻/CD3⁻/NK.1.1⁻/MHCII⁻/CD11c⁻CD11b⁺/Ly6G⁻/Ly6C^{low or high}. Eosinophils were identified as F/480⁻B220⁻/CD3⁻/NK.1.1⁻/MHCII⁻/CD11c⁻CD11b⁺/Ly6G⁻/Ly6C^{med}. For the detection of phosphorylated S235/236 of S6 with intracellular staining, cell suspensions were fixed and permeabilized using the Cytofix-Cytoperm and Cytoperm-Wash buffers (*BD Biosciences*, #554714) and subsequently stained for 120min at RT.

To investigate the hematopoietic stem cell populations in the bone marrow (BM), cells were collected from one femur and one tibiae. LT-HSCs were identified as Lineage⁻/IL7ra⁻/cKIT⁺/Sca1⁺/CD150⁺/CD48⁻. MPP1 cells were identified as Lineage⁻/IL7ra⁻/cKIT⁺/Sca1⁺/CD150⁻/CD48⁻. MPP2 cells were identified as Lineage⁻/IL7ra⁻/cKIT⁺/Sca1⁺/CD150⁺/CD48⁺. MPP3/4 cells were identified as Lineage⁻/IL7ra⁻/cKIT⁺/Sca1⁺/CD150⁻/CD48⁺. GMP cells were identified as Lineage⁻/IL7ra⁻/cKIT⁺/Sca1⁻/FcγRIIb⁺/CD34⁺. CMP cells were identified as Lineage⁻/IL7ra⁻/cKIT⁺/Sca1⁻/FcγRIIb^{lo}/CD34⁺. MEP cells were identified as Lineage⁻/IL7ra⁻/cKIT⁺/Sca1⁻/FcγRIIb⁻/CD34⁻.

All flow cytometry analyses were done at the Flow Cytometry Facility (CNIO), using BD LSR-Fortessa or BD CantoB cell analyzers, running BD FACSDiva software (BD Biosciences). FlowJo software (v 9.8.1 and v.10; TreeStar) was used for data analyses and plot rendering. See details on the gating strategies in Data S1.

Immunoblotting—Cells were rinsed once with ice-cold PBS and lysed in ice-cold lysis buffer (50 mM HEPES [pH 7.4], 40mM NaCl, 2mM EDTA, 1.5mM sodium orthovanadate, 50mM NaF, 10mM pyrophosphate, 10mM glycerophosphate, and 1% Triton X-100, and one tablet of EDTA-free complete protease inhibitors [Roche] per 25ml). Cell lysates were cleared by centrifugation at 13,000rpm for 10 min. Proteins extracts were denatured by the addition of sample buffer, boiled for 5min, resolved by SDS-PAGE, and analyzed by immunoblotting. Western blot analyses were performed according to standard procedures.

RNA extraction, cDNA synthesis and qRT-PCR—Total RNA was extracted from tissues or cells with TRIzol (Invitrogen, #15596026) according to manufacturer's instructions. Isolated RNA was treated with DNase (QIAGEN, #79254) prior to cDNA synthesis. To perform cDNA synthesis, 1ug of RNA was retrotranscribed using SuperScript

IV VILO Master Mix (Invitrogen, #11756500) following manufacturer's instructions. Quantitative real time-PCR was performed using GoTaq® qPCR Master Mix (Promega #6001) in an QuantStudio 6 Flex Real-Time PCR System thermocycler (Applied Biosystems). Data were analyzed by the change-in-threshold (2^{-CT}) method, using β -actin as “housekeeping” reference gene. Results are represented as fold changes relative to the mean expression levels of the wild-type mice. Primers were designed using Primer3 Software (<https://bioinfo.ut.ee/primer3-0.4.0/>).

Gene expression profiling of GC B cells and FL—GC B cells (CD19⁺, CD95⁺, CD38⁻) were sorted from RagC^{Q119L/+} and RagC^{+/+} splenocytes after 12 d of SRBC immunization in a BD FACSAria IIu (Becton Dickinson) and InFlux (Cytocopia-Becton Dickinson) cell sorters. For gene expression profiling of murine lymphomas, B220⁺ cells were isolated from mouse lymphoma tumors by immunomagnetic enrichment with CD45R (B220) microbeads (Miltenyi Biotech, #130-049-501).

Total RNA from sorted cells was extracted using TRIzol and PicoPure RNA Isolation kit (Arcturus, #12204-01) following the manufacturer's instructions.

Total RNA samples were processed into cDNA sequencing libraries with the “QuantSeq 3' mRNA-Seq Library Prep Kit (FWD) for Illumina” (Lexogen, Cat.No. 015). Library generation is initiated by reverse transcription with oligodT priming, followed by a random-primed second strand synthesis. Primers from both steps contain Illumina-compatible sequences. Libraries are completed by PCR, and sequenced on an Illumina NextSeq 550 (with v2.5 reagent kits) by following manufacturer's protocols. This library preparation kit generates directional libraries stranded in the sense orientation: the read1 (the only read in single read format) has the sense orientation. Eighty six-base-pair single-end sequenced reads followed adaptor and polyA tail removal as indicated by Lexogen. 20–25 million reads per sample were analyzed with the nextpresso (Graña et al., 2017) pipeline as follows: sequencing quality was checked with FastQCv0.11.0 (<https://www.bioinformatics.babraham.ac.uk/projects/fastqc/>). Reads were aligned to the mouse genome (GRCm38) with TopHat2 (Trapnell et al., 2012) using Bowtie (Langmead et al., 2009) and Samtools (Li et al., 2009), allowing 3 mismatches and 20 multi hits. The Gencode vM25 gene annotation for GRCm38 was used. Read counts were obtained with HTSeq (Anders et al., 2015). Differential expression and normalization was performed with DESeq2 (Love et al., 2014), keeping only those genes where the normalized count value was higher than 2 in at least 10% of the samples. Finally, those genes that had an adjusted p value below 0.05 FDR were selected. GSEA Preranked (Subramanian et al., 2005) was used to perform gene set enrichment analysis for the selected gene signatures on a pre-ranked gene list, setting 1000 gene set permutations. Only those gene sets with significant enrichment levels (FDR q-value < 0.05) were considered.

Diagnose of murine lymphomas and autoimmunity—Lymphoproliferative diseases developing in the VavP-Bcl2^{tg}; RagC^{Q119L/+} cohort were diagnosed based on morphology according to the following criteria, in analogy to the classification of human lymphoma: (i) early stages of FL (FL *in situ*), defined by the presence of oversized follicles with partial or absent mantle zone and loss of confinement in the context of a yet preserved tissue

architecture; (ii) overt FL of various grades, characterized by the effacement of the nodal and/or splenic architecture by a proliferation of follicle center B cells with a follicular growth pattern occupying the medullary and/or paracortical areas; (iii) DLBCL, defined by the effacement of the lymphoid organ architecture due to the expansion of large cells, with occasional infiltration beyond the capsule into surrounding soft tissues (Zhang et al., 2017). FL was classified into the following three histological grades: grade I, 0-5 centroblasts in 40x field; grade II, 6-15 centroblasts in 40x field; grade III, > 15 centroblasts in 40x field. Lymph nodes, spleen, BM and other tissues with abnormal mononuclear infiltrate were evaluated. Mice showing numerous grossly enlarged and fused germinal centers replete with more than 5 germinal centers per nodule of white pulp in the spleen were considered lymphoma. Bcl6 stain was used in doubtful cases to highlight the follicular pattern. The genotype of the animal was not disclosed to the pathologist (E. Caleiras). Autoimmunity was scored by perivascular inflammatory infiltrate, predominantly mononuclear of lymphoid aspect, with or without necrosis of the vessel wall, and was most prevalently seen in salivary glands and kidney. Autoimmune glomerulonephritis was defined by hypercellular glomeruli containing eosinophilic deposits, generally accompanied by Bowman epithelium hyperproliferation

Histological and immunohistochemical analysis of mouse tissues—Tissue samples were fixed in 10% neutral buffered formalin (4% formaldehyde in solution), paraffin-embedded and cut at 3 μ m, mounted in superfrost®plus slides and dried overnight. For different staining methods, slides were deparaffinized in xylene and re-hydrated through a series of graded ethanol until water. Consecutive sections were stained with hematoxylin and eosin (H&E), and several immunohistochemistry reactions were performed in an automated immunostaining platform (Ventana Discovery XT). Antigen retrieval was first performed with the appropriate pH buffer, (CC1m, Ventana, Roche) and endogenous peroxidase was blocked (peroxide hydrogen at 3%). Then, slides were incubated with the appropriate primary antibody as detailed: mouse monoclonal anti-Bcl6 (1/30 dilution; CNIO Monoclonal Antibodies Core Unit #AM191E/A8), anti-Ki67 (clone D3B5, Cell Signaling Technology, #12202), After the primary antibody, slides were incubated with the visualization systems (Omni Map anti-Rabbit, Ventana, Roche) conjugated with horseradish peroxidase. Immunohistochemical reaction was developed using 3, 30-diaminobenzidine tetrahydrochloride (DAB) (Chromo Map DAB, Ventana, Roche; DAB Dako) and nuclei were counterstained with Carazzi's hematoxylin. Finally, the slides were dehydrated, cleared and mounted with a permanent mounting medium for microscopic evaluation. Positive control sections known to be primary antibody positive were included for each staining run. For KI67 quantification, whole slides were acquired with a slide scanner (AxioScan Z1, Zeiss). After ROI (Regions Of Interest) selection (lymph nodes and spleen), areas for quantification were selected and exported as subsets of images in TIFF format. All images were then checked and those with staining or cutting artifacts were eliminated. Different images from different slides were chosen for quantification program training (AxioVision 4.6 software package, Zeiss) and an appropriate script for KI67 quantification was created: positivity was evaluated in one phase (phase 1, positive cells) and compared with tumor area (phase 2, tumor area). After training and script optimization, the quantification program was

run and results exported as excel files with scoring data for each TIFF file. Data obtained was then compiled and appropriately assessed.

QUANTIFICATION AND STATISTICAL ANALYSIS

The n, indicating the total number of animals per group, as well as the definition of center, dispersion and precision measures are indicated in each Figure and Figure legend. Unless otherwise stated, two-tailed Student's t test or Chi square test were performed as depicted in the Figures. Survival in mouse experiments was represented with Kaplan–Meier curves, and significance was estimated with the log-rank test. Statistical analyses were performed with Prism 9 software (GraphPad).

Supplementary Material

Refer to Web version on PubMed Central for supplementary material.

ACKNOWLEDGMENTS

We are indebted to D.M. Sabatini (NIH grants R01 CA129105, R01 CA103866, and R37 AI047389) and thank R. Jaenisch, S. Markoulaki, and the Whitehead Institute for Biomedical Research CRISPR facility for zygote injections. We thank the CNIO Flow Cytometry, Histopathology, Animal Facility and Genomics Core Units for excellent technical support. Research was supported by the RETOS Projects Program of the Spanish Ministry of Science, Innovation and Universities, the Spanish State Research Agency (AEI/10.13039/501100011033) co-funded by the European Regional Development Fund (SAF2015-67538-R and PID2019-104012RB-I00), the EU-H2020 Program (ERC-2014-STG-638891), an Excellence Network Grant from MICIU/AEI (SAF2016-81975-REDT), a Ramon y Cajal Award from MICIU/AEI (RYC-2013-13546), a Spanish Association Against Cancer Research Scientific Foundation laboratory grant (LABAE16001EFEY/AECC), Beca de Investigación en Oncología Olivia Roddom, a FERO Grant for Research in Oncology. This work was also supported by a Miguel Servet fellowship and grant award (MS16/00112 and CP16/00112) and Project PI18/00816 within the Health Strategic Action from the Instituto de Salud Carlos III (ISCIII) (to A.O.-M.), both co-funded by the European Regional Development Fund. The CNIO Bioinformatics Unit is supported by ISCIII a Spanish National Bioinformatics Institute (ELIXIR-ES, INB) grant (PT17/0009/0011-ISCIII-SGEFI/ERDF-EU). N.D.-S. and A.B.P.-G. are recipients of Ayudas de contratos predoctorales para la formación de doctores from MICIU/AEI (BES-2016-077410 and BES-2017-081381). A.E. is an EMBO Young Investigator. A.E. dedicates this work to the memory of Diego Armando Maradona.

REFERENCES

- Anders S, Pyl PT, and Huber W (2015). HTSeq—a Python framework to work with high-throughput sequencing data. *Bioinformatics* 31, 166–169. [PubMed: 25260700]
- Anderson RM, Le Couteur DG, and De Cabo R (2018). Caloric restriction research: New perspectives on the biology of aging. *J. Gerontol. A Biol. Sci. Med. Sci* 73, 1–3.
- Bannard O, and Cyster JG (2017). Germinal centers: programmed for affinity maturation and antibody diversification. *Curr. Opin. Immunol* 45, 21–30. [PubMed: 28088708]
- Béguelin W, Popovic R, Teater M, Jiang Y, Bunting KL, Rosen M, Shen H, Yang SN, Wang L, Ezponda T, et al. (2013). EZH2 is required for germinal center formation and somatic EZH2 mutations promote lymphoid transformation. *Cancer Cell* 23, 677–692. [PubMed: 23680150]
- Bellantuono I, de Cabo R, Ehninger D, Di Germanio C, Lawrie A, Miller J, Mitchell SJ, Navas-Enamorado I, Potter PK, Tchkonja T, et al. (2020). A toolbox for the longitudinal assessment of healthspan in aging mice. *Nat. Protoc* 15, 540–574. [PubMed: 31915391]
- Chung CYS, Shin HR, Berdan CA, Ford B, Ward CC, Olzmann JA, Zoncu R, and Nomura DK (2019). Covalent targeting of the vacuolar H⁺-ATPase activates autophagy via mTORC1 inhibition. *Nat. Chem. Biol* 15, 776–785. [PubMed: 31285595]

- De Cecco M, Ito T, Petrashen AP, Elias AE, Skvir NJ, Criscione SW, Caligiana A, Broccoli G, Adney EM, Boeke JD, et al. (2019). L1 drives IFN in senescent cells and promotes age-associated inflammation. *Nature* 566, 73–78. [PubMed: 30728521]
- de la Calle Arregui C, Plata-Gomez AB, Deleyto-Seldas N, Garcia F, Ortega-Molina A, Abril-Garrido J, et al. (2021). Limited survival and impaired hepatic fasting metabolism in mice with constitutive Rag GTPase signaling. *Nat. Commun* 12, 3660. [PubMed: 34135321]
- Do MH, Wang X, Zhang X, Chou C, Nixon BG, Capistrano KJ, Peng M, Efeyan A, Sabatini DM, and Li MO (2020). Nutrient mTORC1 signaling underpins regulatory T cell control of immune tolerance. *J. Exp. Med* 217, e20190848. [PubMed: 31649036]
- Efeyan A, Zoncu R, Chang S, Gumper I, Snitkin H, Wolfson RL, Kirak O, Sabatini DD, and Sabatini DM (2013). Regulation of mTORC1 by the Rag GTPases is necessary for neonatal autophagy and survival. *Nature* 493, 679–683. [PubMed: 23263183]
- Efeyan A, Schweitzer LD, Bilate AM, Chang S, Kirak O, Lamming DW, and Sabatini DM (2014). RagA, but not RagB, is essential for embryonic development and adult mice. *Dev. Cell* 29, 321–329. [PubMed: 24768164]
- Egle A, Harris AW, Bath ML, O'Reilly L, and Cory S (2004). VavP-Bcl2 transgenic mice develop follicular lymphoma preceded by germinal center hyperplasia. *Blood* 103, 2276–2283. [PubMed: 14630790]
- Ersching J, Efeyan A, Mesin L, Jacobsen JT, Pasqual G, Grabiner BC, Dominguez-Sola D, Sabatini DM, and Victora GD (2017). Germinal Center Selection and Affinity Maturation Require Dynamic Regulation of mTORC1 Kinase. *Immunity* 46, 1045–1058.e6. [PubMed: 28636954]
- Gems D, and Partridge L (2013). Genetics of longevity in model organisms: debates and paradigm shifts. *Annu. Rev. Physiol* 75, 621–644. [PubMed: 23190075]
- Graña O, Rubio-Camarillo M, Fdez-Riverola F, Pisano DG, and Glez-Peña D (2017). Nextpresso: Next Generation Sequencing Expression Analysis Pipeline. *Curr. Bioinform* 13, 583–591.
- Green MR, Kihira S, Liu CL, Nair RV, Salari R, Gentles AJ, Irish J, Stehr H, Vicente-Duerñas C, Romero-Camarero I, et al. (2015). Mutations in early follicular lymphoma progenitors are associated with suppressed antigen presentation. *Proc. Natl. Acad. Sci. USA* 112, E1116–E1125. [PubMed: 25713363]
- Huet S, Sujobert P, and Salles G (2018). From genetics to the clinic: a translational perspective on follicular lymphoma. *Nat. Rev. Cancer* 18, 224–239. [PubMed: 29422597]
- Ingram DK, and de Cabo R (2017). Calorie restriction in rodents: Caveats to consider. *Ageing Res. Rev* 39, 15–28. [PubMed: 28610949]
- Kahl BS, and Yang DT (2016). Follicular lymphoma: evolving therapeutic strategies. *Blood* 127, 2055–2063. [PubMed: 26989204]
- Kalaitzidis D, Lee D, Efeyan A, Kfoury Y, Nayyar N, Sykes DB, Mercier FE, Papazian A, Baryawno N, Victora GD, et al. (2017). Amino acid-insensitive mTORC1 regulation enables nutritional stress resilience in hematopoietic stem cells. *J. Clin. Invest* 127, 1405–1413. [PubMed: 28319048]
- Kang SA, O'Neill DJ, Machl AW, Lumpkin CJ, Galda SN, Sengupta S, Mahoney SJ, Howell JJ, Molz L, Hahn S, et al. (2019). Discovery of Small-Molecule Selective mTORC1 Inhibitors via Direct Inhibition of Glucose Transporters. *Cell Chem. Biol.* 26, 1203–1213.e13. [PubMed: 31231029]
- Kim YC, Park HW, Sciarretta S, Mo JS, Jewell JL, Russell RC, Wu X, Sadoshima J, and Guan KL (2014). Rag GTPases are cardioprotective by regulating lysosomal function. *Nat. Commun* 5, 4241. [PubMed: 24980141]
- Kitamura D, Roes J, Kühn R, and Rajewsky K (1991). A B cell-deficient mouse by targeted disruption of the membrane exon of the immunoglobulin mu chain gene. *Nature* 350, 423–426. [PubMed: 1901381]
- Kridel R, Chan FC, Mottok A, Boyle M, Farinha P, Tan K, Meissner B, Bashashati A, McPherson A, Roth A, et al. (2016). Histological Transformation and Progression in Follicular Lymphoma: A Clonal Evolution Study. *PLoS Med.* 13, e1002197. [PubMed: 27959929]
- Langmead B, Trapnell C, Pop M, and Salzberg SL (2009). Ultrafast and memory-efficient alignment of short DNA sequences to the human genome. *Genome Biol.* 10, R25. [PubMed: 19261174]

- Li H, Handsaker B, Wysoker A, Fennell T, Ruan J, Homer N, Marth G, Abecasis G, and Durbin R; 1000 Genome Project Data Processing Subgroup (2009). The Sequence Alignment/Map format and SAMtools. *Bioinformatics* 25,2078–2079. [PubMed: 19505943]
- Liao CY, Rikke BA, Johnson TE, Diaz V, and Nelson JF (2010). Genetic variation in the murine lifespan response to dietary restriction: from life extension to life shortening. *Aging Cell* 9, 92–95. [PubMed: 19878144]
- Lopez-Guadamillas E, Fernandez-Marcos PJ, Pantoja C, Muñoz-Martin M, Martínez D, Gómez-López G, Campos-Olivas R, Valverde AM, and Serrano M (2016). p21^{Cip1} plays a critical role in the physiological adaptation to fasting through activation of PPAR α . *Sci. Rep* 6, 34542. [PubMed: 27721423]
- López-Otín C, Blasco MA, Partridge L, Serrano M, and Kroemer G (2013). The hallmarks of aging. *Cell* 153, 1194–1217. [PubMed: 23746838]
- Love MI, Huber W, and Anders S (2014). Moderated estimation of fold change and dispersion for RNA-seq data with DESeq2. *Genome Biol.* 15, 550. [PubMed: 25516281]
- Matasar MJ, Luminari S, Barr PM, Barta SK, Danilov AV, Hill BT, Phillips TJ, Jerkeman M, Magagnoli M, Nastoupil LJ, et al. (2019). Follicular Lymphoma: Recent and Emerging Therapies, Treatment Strategies, and Remaining Unmet Needs. *Oncologist* 24, e1236–e1250. [PubMed: 31346132]
- Mesin L, Ersching J, and Victoria GD (2016). Germinal Center B Cell Dynamics. *Immunity* 45, 471–482. [PubMed: 27653600]
- Mitchell SJ, Madrigal-Matute J, Scheibye-Knudsen M, Fang E, Aon M, González-Reyes JA, Cortassa S, Kaushik S, Gonzalez-Freire M, Patel B, et al. (2016). Effects of Sex, Strain, and Energy Intake on Hallmarks of Aging in Mice. *Cell Metab.* 23, 1093–1112. [PubMed: 27304509]
- Okosun J, Wolfson RL, Wang J, Araf S, Wilkins L, Castellano BM, Escudero-Ibarz L, Al Seraihi AF, Richter J, Bernhart SH, et al. (2016). Recurrent mTORC1-activating RRAGC mutations in follicular lymphoma. *Nat. Genet* 48, 183–188. [PubMed: 26691987]
- Ortega-Molina A, Efeyan A, Lopez-Guadamillas E, Muñoz-Martin M, Gómez-López G, Carriamero M, Mulero F, Pastor J, Martinez S, Romanos E, et al. (2012). Pten positively regulates brown adipose function, energy expenditure, and longevity. *Cell Metab.* 15, 382–394. [PubMed: 22405073]
- Ortega-Molina A, Lopez-Guadamillas E, Mattison JA, Mitchell SJ, Muñoz-Martin M, Iglesias G, Gutierrez VM, Vaughan KL, Szarowicz MD, González-García I, et al. (2015). Pharmacological inhibition of PI3K reduces adiposity and metabolic syndrome in obese mice and rhesus monkeys. *Cell Metab.* 21,558–570. [PubMed: 25817535]
- Ortega-Molina A, Deleyto-Seldas N, Carreras J, Sanz A, Lebrero-Fernández C, Menéndez C, Vandenberg A, Fernández-Ruiz B, Marín-Arraiza L, de la Calle Arregui C, et al. (2019). Oncogenic Rag GTPase signaling enhances B cell activation and drives follicular lymphoma sensitive to pharmacological inhibition of mTOR. *Nat. Metab* 1, 775–789. [PubMed: 31579886]
- Sancak Y, Peterson TR, Shaul YD, Lindquist RA, Thoreen CC, Bar-Peled L, and Sabatini DM (2008). The Rag GTPases bind raptor and mediate amino acid signaling to mTORC1. *Science* 320, 1496–1501. [PubMed: 18497260]
- Saxton RA, and Sabatini DM (2017). mTOR Signaling in Growth, Metabolism, and Disease. *Cell* 169, 361–371.
- Saxton RA, Knockenbauer KE, Wolfson RL, Chantranupong L, Pacold ME, Wang T, Schwartz TU, and Sabatini DM (2016). Structural basis for leucine sensing by the Sestrin2-mTORC1 pathway. *Science* 351, 53–58. [PubMed: 26586190]
- Selman C, Tullet JMA, Wieser D, Irvine E, Lingard SJ, Choudhury AI, Claret M, Al-Qassab H, Carmignac D, Ramadani F, et al. (2009). Ribosomal protein S6 kinase 1 signaling regulates mammalian life span. *Science* 326, 140–144. [PubMed: 19797661]
- Sengupta S, Giaime E, Narayan S, Hahm S, Howell J, O’Neill D, Vlasuk GP, and Saiah E (2019). Discovery of NV-5138, the first selective Brain mTORC1 activator. *Sci. Rep* 9, 4107. [PubMed: 30858438]

- Shen K, Choe A, and Sabatini DM (2017). Intersubunit Crosstalk in the Rag GTPase Heterodimer Enables mTORC1 to Respond Rapidly to Amino Acid Availability. *Mol. Cell* 68, 552–565.e8. [PubMed: 29056322]
- Shimobayashi M, and Hall MN (2014). Making new contacts: the mTOR network in metabolism and signalling crosstalk. *Nat. Rev. Mol. Cell Biol* 15, 155–162. [PubMed: 24556838]
- Shlomchik MJ, and Weisel F (2012). Germinal center selection and the development of memory B and plasma cells. *Immunol. Rev* 247, 52–63. [PubMed: 22500831]
- Singh PP, Demmitt BA, Nath RD, and Brunet A (2019). The Genetics of Aging: A Vertebrate Perspective. *Cell* 177, 200–220. [PubMed: 30901541]
- Subramanian A, Tamayo P, Mootha VK, Mukherjee S, Ebert BL, Gillette MA, Paulovich A, Pomeroy SL, Golub TR, Lander ES, and Mesirov JP (2005). Gene set enrichment analysis: a knowledge-based approach for interpreting genome-wide expression profiles. *Proc. Natl. Acad. Sci. USA* 102, 15545–15550. [PubMed: 16199517]
- Tas JMJJ, Mesin L, Pasqual G, Targ S, Jacobsen JT, Mano YM, Chen CSC, Weill J-CJC, Reynaud CAC-A, Browne EPE, et al. (2016). Visualizing antibody affinity maturation in germinal centers. *Science* 351, 1048–1054. [PubMed: 26912368]
- Trapnell C, Roberts A, Goff L, Pertea G, Kim D, Kelley DR, Pimentel H, Salzberg SL, Rinn JL, and Pachter L (2012). Differential gene and transcript expression analysis of RNA-seq experiments with TopHat and Cufflinks. *Nat. Protoc* 7, 562–578. [PubMed: 22383036]
- Valvezan AJ, and Manning BD (2019). Molecular logic of mTORC1 signalling as a metabolic rheostat. *Nat. Metab* 1, 321–333. [PubMed: 32694720]
- Victoria GD, and Nussenzweig MC (2012). Germinal centers. *Annu. Rev. Immunol* 30, 429–457. [PubMed: 22224772]
- Wang H, Yang H, Shivalila CS, Dawlaty MM, Cheng AW, Zhang F, and Jaenisch R (2013). One-step generation of mice carrying mutations in multiple genes by CRISPR/Cas-mediated genome engineering. *Cell* 153, 910–918. [PubMed: 23643243]
- Whittemore K, Derevyanko A, Martinez P, Serrano R, Pumarola M, Bosch F, and Blasco MA (2019). Telomerase gene therapy ameliorates the effects of neurodegeneration associated to short telomeres in mice. *Aging (Albany NY)* 11, 2916–2948. [PubMed: 31140977]
- Wu JJ, Liu J, Chen EB, Wang JJ, Cao L, Narayan N, Fergusson MM, Rovira II, Allen M, Springer DA, et al. (2013). Increased mammalian lifespan and a segmental and tissue-specific slowing of aging after genetic reduction of mTOR expression. *Cell Rep.* 4, 913–920. [PubMed: 23994476]
- Ying ZX, Jin M, Peterson LF, Bernard D, Saiya-Cork K, Yildiz M, Wang S, Kaminski MS, Chang AE, Klionsky DJ, and Malek SN (2016). Recurrent mutations in the MTOR regulator RRAGC in follicular lymphoma. *Clin. Cancer Res* 22, 5383–5393. [PubMed: 27267853]
- Zhang J, Vlasevska S, Wells VA, Nataraj S, Holmes AB, Duval R, Meyer SN, Mo T, Basso K, Brindle PK, et al. (2017). The CREBBP acetyltransferase is a haploinsufficient tumor suppressor in B-cell lymphoma. *Cancer Discov.* 7, 322–337. [PubMed: 28069569]
- Zoncu R, Efeyan A, and Sabatini DM (2011). mTOR: from growth signal integration to cancer, diabetes and ageing. *Nat. Rev. Mol. Cell Biol* 12, 21–35. [PubMed: 21157483]

Highlights

- Knockin mice expressing a hypomorphic form of the RagC GTPase (Q119L) are viable
- *RagC*^{Q119L/+} mice show attenuated nutrient signaling-mTORC1 activity
- Lymphomagenesis and self-reactivity are delayed when induced in *RagC*^{Q119L/+} mice
- Aside from B cells, *RagC*^{Q119L/+} mice show minimal defects and a normal lifespan

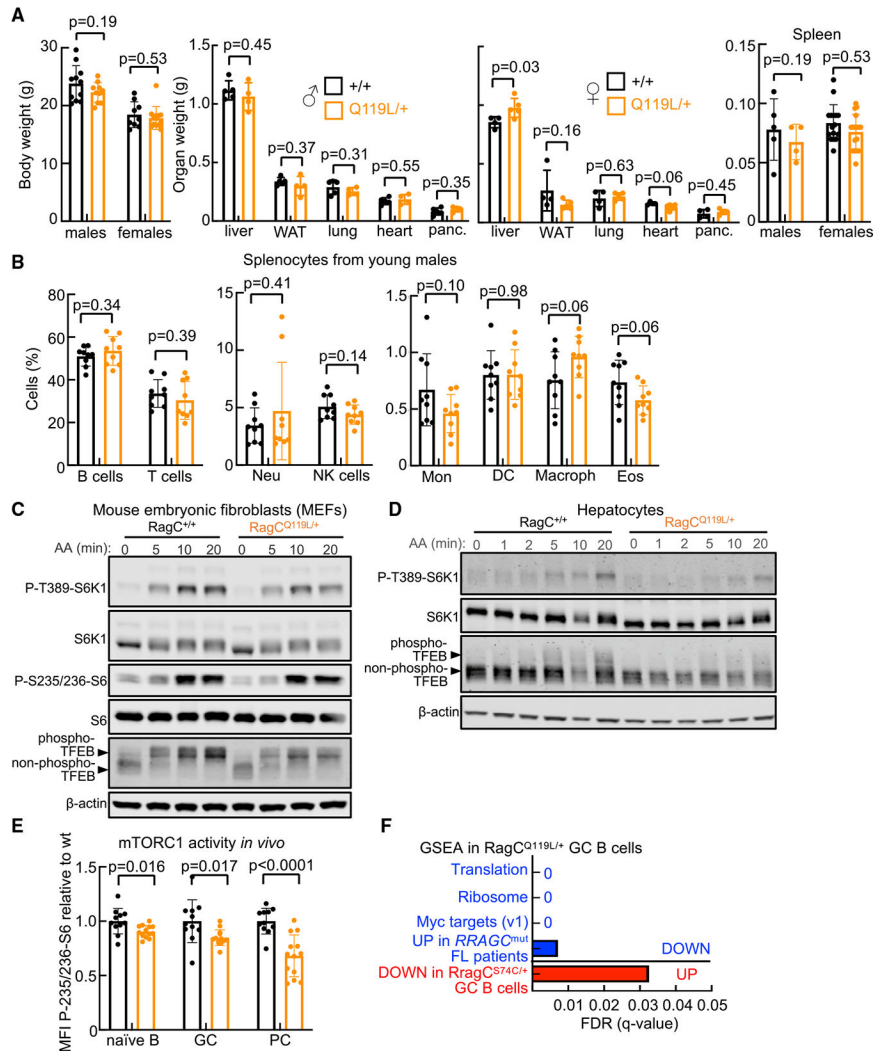


Figure 1. RagC^{Q119L/+} knockin mice show a mild reduction in mTORC1 activity *in vitro* and *in vivo*

(A) Left: body weight of RagC^{+/+} (n = 11) and RagC^{Q119L/+} (n = 10) males, and RagC^{+/+} (n = 9) and RagC^{Q119L/+} (n = 12) females. Center: tissue weights of RagC^{+/+} (n = 5) and RagC^{Q119L/+} (n = 4) males and RagC^{+/+} (n = 4) and RagC^{Q119L/+} (n = 5) females. Right: spleen weights of RagC^{+/+} (n = 5) and RagC^{Q119L/+} (n = 4) males and RagC^{+/+} (n = 16) and RagC^{Q119L/+} (n = 17) females. All mice were 7–8 week old.

(B) Percentage of the indicated cell populations in the spleen of 2- to 3-month-old RagC^{+/+} (n = 9) and RagC^{Q119L/+} (n = 9) males. Neu, neutrophil; Mon, monocyte; NK, natural killer; Eos, eosinophil; DC, dendritic cell; Macroph, macrophage.

(C) MEFs from RagC^{+/+} and RagC^{Q119L/+} mice were deprived of all amino acids in RPMI medium for 45 min and re-stimulated with amino acids for 5, 10, and 20 min.

(D) Primary hepatocytes from RagC^{+/+} and RagC^{Q119L/+} females were deprived of all amino acids in DMEM/F12 for 1 h and re-stimulated with amino acids for the indicated times.

(C and D) Whole-cell protein lysates were immunoblotted for the indicated proteins.

(E) Quantification of mTORC1 activity in naive B cells (B220⁺ GL7⁻CD95⁻), GC B cells (B220⁺ gated, GL7⁺, and CD95⁺), and PCs (B220^{low} and CD138⁺ gated), revealed by intracellular phospho-S6 staining 10 days after immunization with SRBCs of 7- to 8-week-old RagC^{+/+} (n = 11) and RagC^{Q119L/+} (n = 13) mice. MFI, median fluorescence intensity.

(F) Graphical representation of the false discovery rates (FDRs) from the indicated KEGG, Hallmark, REACTOME, and curated gene sets depleted (blue) and enriched (red) in RagC^{Q119L/+} (n = 4) versus RagC^{+/+} (n = 4) GC B cells.

Bars in (A), (B), and (E) indicate the mean ± SD. Statistical significance in (A), (B), and (E) was calculated by two-tailed Student's t test.

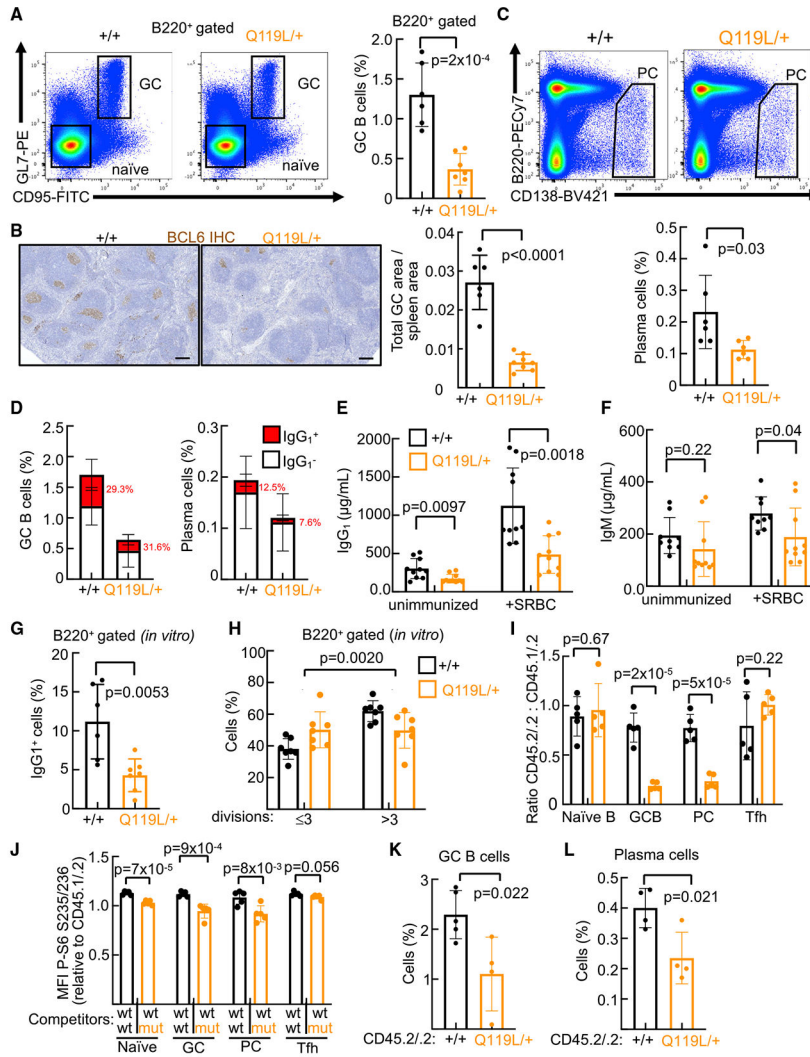


Figure 2. Diminished humoral response in RagC^{Q119L/+} mutant mice
 (A) Representative flow cytometry plots (left; B220⁺ gated, GL7⁺, and CD95⁺) and their quantification (right) of GC B cells in spleens harvested from 7- 13-week-old RagC^{+/+} (n = 6) and RagC^{Q119L/+} (n = 7) females 10 days after immunization with SRBCs.
 (B) Immunohistochemistry (IHC) staining of anti-Bcl6 (left) and quantification of GC area (right) in spleens harvested from immunized 7- to 8-week-old RagC^{+/+} and RagC^{Q119L/+} mice. Scale bar, 200 μ m.
 (C) Representative flow cytometry plots (top; B220^{low} and CD138⁺) and quantification (bottom) of PCs from 7- to 13-week-old RagC^{+/+} (n = 6) and RagC^{Q119L/+} (n = 6) females 10 days after immunization.
 (D) Quantification of IgG₁⁺ cells in GC B cells (left) and PCs (right) in spleens harvested from 7- to 13-week-old RagC^{+/+} (n = 8) and RagC^{Q119L/+} (n = 12) mice 10 days after immunization.
 (E and F) IgG₁ (E) and IgM (F) quantification of sera from RagC^{+/+} (n = 10) and RagC^{Q119L/+} (n = 10) females before and 10 days after immunization, measured by ELISA.
 (G) B220⁺ gated (in vitro) IgG₁⁺ cells (%).
 (H) B220⁺ gated (in vitro) Cells (%).
 (I) Ratio CD45.2/2 : CD45.1/2 in Naive B, GCB, PC, and Tfh cells.
 (J) MFI of S6 S225/236 (relative to CD45.1/2) in Naive, GC, PC, and Tfh cells.
 (K) GC B cells.
 (L) Plasma cells.

(G) *In vitro* IgG₁ CSR in B220⁺ cells from 2- to 4-month-old RagC^{+/+} (n = 5) and RagC^{Q119L/+} (n = 7) mice 4 days after stimulation with anti-CD40 and IL-4.

(H) Proliferation by CFSE decay in CD43⁻ cells isolated from 2- to 3.5-month-old RagC^{+/+} (n = 7) and RagC^{Q119L/+} (n = 7) mice labeled with CFSE dye and cultured in the presence of anti-CD40 and IL-4 for 3 days. (B220⁺ gated).

(I and J) Quantification of CD45.2/.2:CD45.1/.2 ratio (I) and phosphorylation (J) of S6 (S235/236) in naive B cells (B220⁺CD95⁻GL7⁻ gated), GC B cells (B220⁺CD95⁺GL7⁺ gated), PCs (B220^{low}CD138⁺ gated), and Tfh cells (CD4⁺PD1⁺CXCR5⁺ gated) in splenocytes harvested from mixed BM chimeras 10 days after immunization (n = 5 mice per genotype).

(K and L) Quantification of CD45.2/.2 gated GC B cells (B220⁺CD95⁺GL7⁺) (K) and PCs (B220^{low}CD138⁺) (L) in spleens collected from Ighm^{μMT/μMT}:RagC^{+/+} or Ighrn^{μMT/μMT}:RagC^{Q119L/+} mice 10 days after immunization (n = 4 mice per genotype). Bars indicate the mean ± SD. Statistical significance in (A)–(I) and (J)–(L) was calculated by two-tailed Student's t test. Statistical significance in (H) was determined using two-way ANOVA.

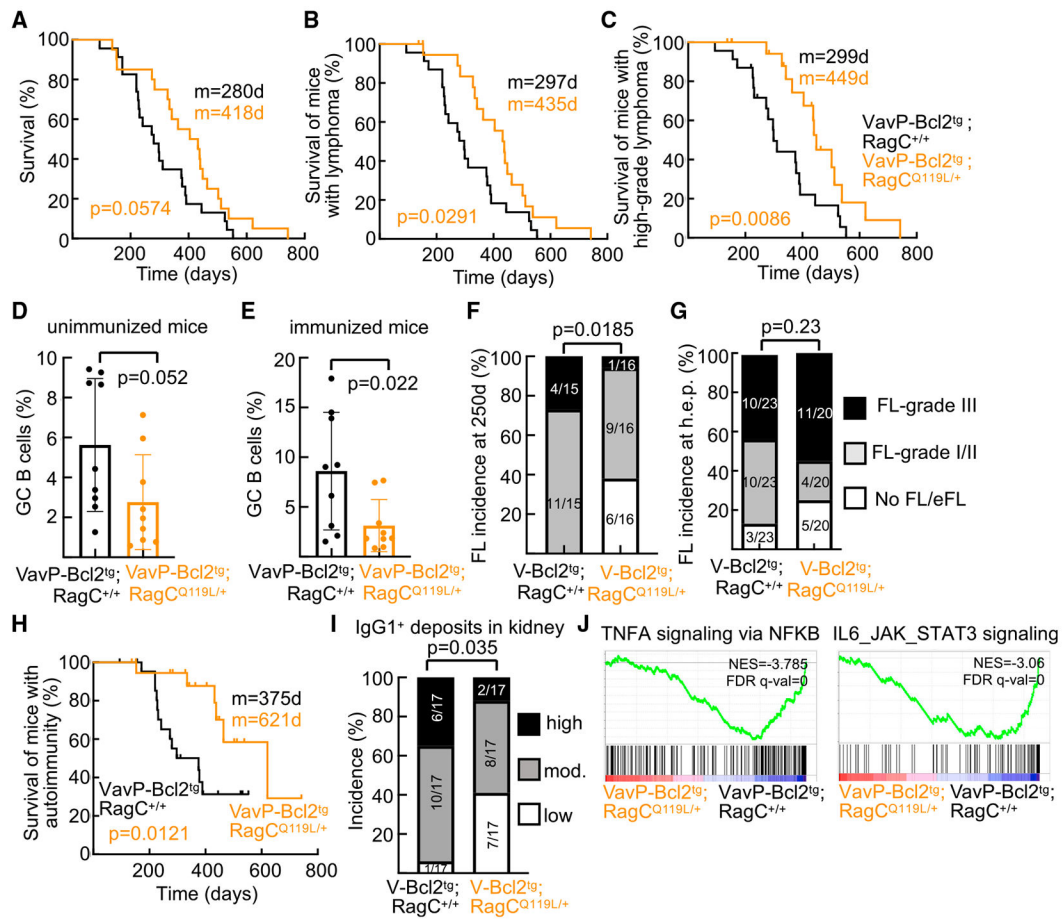


Figure 3. Delayed lymphomagenesis by heterozygous expression of mutant RagC Q119L in mice (A) Kaplan-Meier survival curve of VavP-Bcl2^{tg}; RagC^{+/+} (n = 23) and VavP-Bcl2^{tg}; RagC^{Q119L/+} (n = 20) mice.

(B) Kaplan-Meier lymphoma survival curve of VavP-Bcl2^{tg}; RagC^{+/+} (n = 23) and VavP-Bcl2^{tg}; RagC^{Q119L/+} (n = 20) mice. All mice that developed FL were scored as 1.

(C) Kaplan-Meier high-grade lymphoma survival curve of VavP-Bcl2^{tg}; RagC^{+/+} (n = 23) and VavP-Bcl2^{tg}; RagC^{Q119L/+} (n = 20) mice. FL grade II, FL grade III, and diffused tumors were scored as 1, and mice bearing no FL, early FL, and FL grade I were scored as 0.

(D and E) Quantification of GC B cells in spleens harvested from unimmunized (D) and SRBC-immunized (E) RagC^{+/+} (n = 9 and 9) and RagC^{Q119L/+} (n = 9 and 9) mice.

(F) Incidence of FL in VavP-Bcl2^{tg}; RagC^{+/+} (n = 15) and VavP-Bcl2^{tg}; RagC^{Q119L/+} (n = 16) mice sacrificed at 250 days.

(G) Incidence of FL in cohorts at the humane endpoint (h.e.p.) shown in (B).

(H) Kaplan-Meier autoimmunity survival curves of VavP-Bcl2^{tg}; RagC^{+/+} (n = 23) and VavP-Bcl2^{tg}; RagC^{Q119L/+} (n = 20) mice. All mice that developed autoimmunity were scored as 1.

(I) Quantification of IgG₁⁺ deposits in kidneys of VavP-Bcl2^{tg}; RagC^{+/+} (n = 17) and VavP-Bcl2^{tg}; RagC^{Q119L/+} (n = 17) mice.

(J) Enrichment of gene signatures related to genes involved in NF- κ B signaling (left) and JAK-STAT signaling (right) in VavP-Bcl2^{tg}; RagC^{+/+} (n = 4) versus VavP-Bcl2^{tg}; RagC^{Q119L/+} (n = 5) FL B220⁺ sorted cells.

Statistical significance in (A)–(C) and (H) was calculated with a log-rank test. Statistical significance in (D) and (E) was calculated by two-tailed Student's t test and in (F), (G), and (I) by Chi-square test. In (A-C) and (H): m, median survival

Author Manuscript

Author Manuscript

Author Manuscript

Author Manuscript

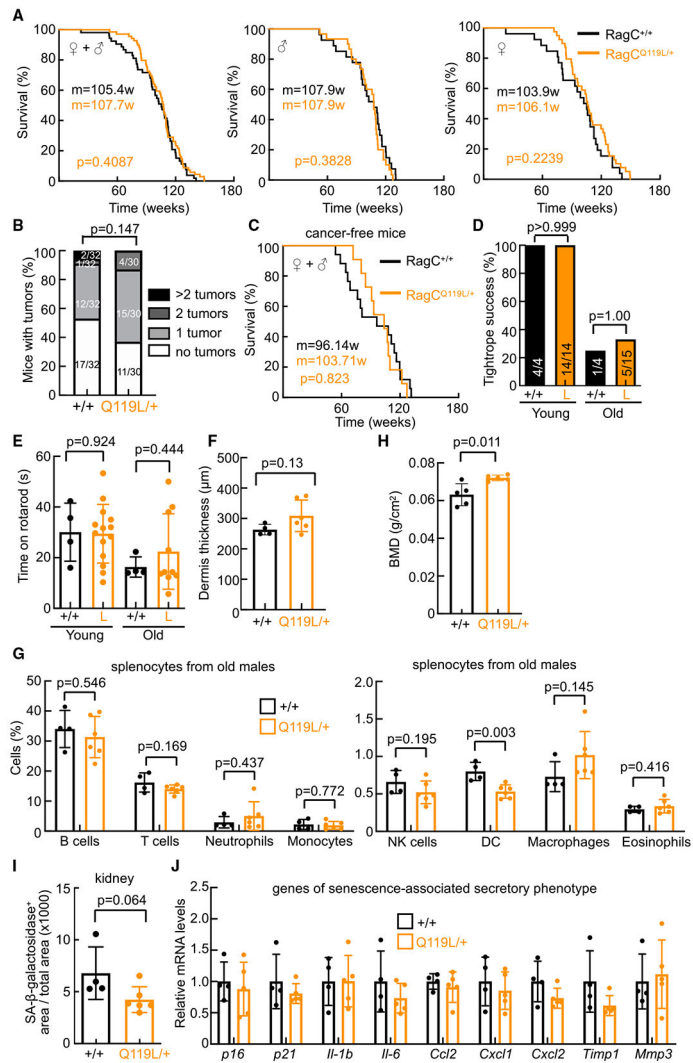


Figure 4. RagC^{Q119L/+} mice have a normal lifespan

(A) Kaplan-Meier survival curves of RagC^{+/+} (n = 53) and RagC^{Q119L/+} (n = 69) mice (left), RagC^{+/+} (n = 27) and RagC^{Q119L/+} (n = 30) males (center), and RagC^{+/+} (n = 26) and RagC^{Q119L/+} (n = 39) females (right).

(B) Percentage of mice with no tumors, one malignant tumor, 2 tumors, and more than 2 tumors (from A).

(C) Kaplan-Meier survival curve of RagC^{+/+} (n = 17) and RagC^{Q119L/+} (n = 11) mice that were free of detectable malignant tumors at the time of death.

(D) Tightrope assay in 5-month-old (young) and 16- to 25-month-old RagC^{+/+} and RagC^{Q119L/+} mice.

(E) Time on the rotarod test, measured in the same mice as in (D).

(F) Dermal thickness in back skin from 25-month-old RagC^{+/+} (n = 4) and RagC^{Q119L/+} (n = 6) males.

(G) Percentage of the indicated cell populations in spleens of 25-month-old RagC^{+/+} (n = 4) and RagC^{Q119L/+} (n = 6) males.

(H) Bone mineral density (BMD) measured in 17- to 25-month-old RagC^{+/+} (n = 5) and RagC^{Q119L/+} (n = 5) males.

(I) Quantification of senescence associated- β -galactosidase (SA- β -gal)⁺ area within the kidney area of the mice shown in (H).

(J) qRT-PCR analysis of senescence-associated secretory phenotype (SASP) genes in the kidneys of the mice in (H) Statistical significance was determined using the Holm-Sidak method, with $\alpha = 0.05$.

Statistical significance in (A) and (C) was calculated with a log rank test, in (B) by Chi-square test, in (D) by two-sided Fisher's exact test, and in (E)–(I) by two-tailed Student's t test. Bars in (E)–(J) indicate the mean \pm SD.

KEY RESOURCES TABLE

REAGENT or RESOURCE	SOURCE	IDENTIFIER
Antibodies		
PE-Cy7 Rat Anti-Mouse CD45R/B220	BD Biosciences	Clone RA3-6B2; Cat#561881; RRID:AB_10893024
BUV737 Rat Anti-Mouse CD45R/B220	BD Biosciences	Clone RA3-6B2; Cat#564449; RRID:AB_2738813
APC Rat Anti-Mouse CD45R/B220	BD Biosciences	Clone RA3-6B2; Cat#553092; RRID:AB_398531
PE Rat Anti-Mouse CD19	BD Biosciences	Clone 1D3; Cat#557399; RRID:AB_396682
BV786 Rat Anti-Mouse CD19	BD Biosciences	Clone 1D3; Cat#563333; RRID:AB_2738141
PE Rat Anti-Mouse T- and B Cell Activation Antigen	BD Biosciences	Clone GL7; Cat#561530; RRID:AB_10715834
FITC Hamster Anti-Mouse CD95	BD Biosciences	Clone Jo2; Cat#561979; RRID:AB_10892808
BV421 Rat Anti-Mouse CD138	BD Biosciences	Clone 281-2; Cat#562610; RRID:AB_11153126
CD38 Monoclonal Antibody, Alexa Fluor 700	Thermo Fisher Scientific	Clone 90; Cat#56-0381-82; RRID:AB_657740
CD184 (CXCR4) Monoclonal Antibody, PE	Thermo Fisher Scientific	Clone 2B11; Cat#12-9991-82; RRID:AB_891391
PE-Cy7 Rat Anti-Mouse CD86	BD Biosciences	Clone GL1; Cat#560582; RRID:AB_1727518
CD4 Monoclonal Antibody, FITC	Thermo Fisher Scientific	Clone GK1.5; Cat#11-0041-81; RRID:AB_464891
PE-Cy7 Rat Anti-CD11b	BD Biosciences	Clone M1/70; Cat#561098; RRID:AB_2033994
F4/80 Monoclonal Antibody, APC-eFluor 780	Thermo Fisher Scientific	Clone BM8; Cat#47-4801-80; RRID:AB_2637188
BUV395 Hamster Anti-Mouse CD3e	BD Biosciences	Clone 145-2C11; Cat#563565; RRID:AB_2738278
PE Anti-Mouse NK1.1 (CD161)	Tonbo Biosciences	Clone PK136; Cat#50-5941; RRID:AB_2621804
FITC Anti-Mouse MHC Class II (I-A/I-E)	Tonbo Biosciences	Clone M5/114.15.2; Cat#35-5321; RRID:AB_2621715
APC Anti-Mouse CD11c	Tonbo Biosciences	Clone N418; Cat#20-0114; RRID:AB_2621557
PerCP-Cyanine5.5 Anti-Mouse Ly-6G	Tonbo Biosciences	Clone 1A8; Cat#65-1276; RRID:AB_2621899
Alexa Fluor700 anti-mouse Ly-6C Antibody	Biolegend	Clone HK1.4; Cat#128024; RRID:AB_10643270
PerCP-Cy5.5 Mouse Lineage Antibody Cocktail	BD Biosciences	Cat#561317; RRID:AB_10612020
APC/Cyanine7 anti-mouse CD117 (c-kit) Antibody	Biolegend	Clone 2B8; Cat#105826; RRID:AB_1626278
Pacific Blue anti-mouse Ly-6A/E (Sca-1) Antibody	Biolegend	Clone E13-161.7; Cat#122520; RRID:AB_2143237
APC anti-mouse CD150 (SLAM) Antibody	Biolegend	Clone TC15-12F12.2; Cat#115910; RRID:AB_493460
PE Hamster Anti-Mouse CD48	BD Biosciences	Clone HM48.1; Cat#557485; RRID:AB_396725

REAGENT or RESOURCE	SOURCE	IDENTIFIER
BUV737 Rat Anti-Mouse CD127	BD Biosciences	Clone SB/199; Cat#612841; RRID:AB_2870163
CD34 Monoclonal Antibody, FITC	Thermo Fisher Scientific	Clone RAM34; Cat#11-0341-82; RRID:AB_465021
PE-Cy7 Rat Anti-Mouse CD16/CD32	BD Biosciences	Clone 2.4G2; Cat#560829; RRID:AB_10563207
Phospho-S6 Ribosomal Protein (Ser235/236) Rabbit mAb (Alexa Fluor® 647 Conjugate)	Cell Signaling Technology	Clone D57.2.2E; Cat#4851; RRID:AB_10695457
APC Rat anti-Mouse IgG1	BD Biosciences	Clone A85-1; Cat#560089; RRID:AB_1645625
CD45.1 Monoclonal Antibody, PerCP-Cyanine5.5	Thermo Fisher Scientific	Clone A20; Cat#45-0453-82; RRID:AB_1107003
CD45.2 Monoclonal Antibody, APC	Thermo Fisher Scientific	Clone 104; Cat#17-0454-81; RRID:AB_469399
APC/Cyanine7 anti-mouse CD45.2 Antibody	Biolegend	Clone 104; Cat#109824; RRID:AB_830789
Biotin Rat Anti-Mouse CD185 (CXCR5)	BD Biosciences	Clone 2G8; Cat#551960; RRID:AB_394301
PE Streptavidin-Phycoerythrin antibody	BD Biosciences	Cat#554061; RRID:AB_10053328
CD279 (PD-1) Monoclonal Antibody, PE-Cyanine7	Thermo Fisher Scientific	Clone J43; Cat#25-9985-80; RRID:AB_10853672
Phospho-p70 S6 Kinase (Thr389) Rabbit mAb	Cell Signaling Technology	Clone 108D2; Cat#9234; RRID:AB_2269803
p70 S6 Kinase Rabbit mAb	Cell Signaling Technology	Clone 49D7; Cat#2708; RRID:AB_390722
CD4 Monoclonal Antibody, FITC	Thermo Fisher Scientific	Clone GK1.5; Cat#11-0041-81; RRID:AB_464891
BUV395 Rat Anti-Mouse CD4	BD Biosciences	Clone GK1.5; Cat#563790; RRID:AB_2738426
APC-Cyanine7 Anti-Human/Mouse CD44	Tonbo Biosciences	Clone IM7; Cat#25-0441; RRID:AB_2621628
PE Rat Anti-Mouse CD62L	BD Biosciences	Clone MEL-14; Cat#553151; RRID:AB_394666
PE-Cy7 Hamster Anti-Mouse CD69	BD Biosciences	Clone H1.2F3; Cat#552879
PerCP-Cy5.5 Rat Anti-Mouse CD25 .	BD Biosciences	Clone PC61; Cat#551071; RRID:AB_394031
Mouse CD40/TNFRSF5 Antibody	R&D Systems	Cat#MAB440; RRID:AB_358378
<i>In Vivo</i> Ready Anti-Mouse CD3e	Tonbo Biosciences	clone 145-2C11; Cat#40-0031; RRID:AB_2621436
<i>In Vivo</i> Ready Anti-Mouse CD28	Tonbo Biosciences	clone 37.51; Cat#40-0281; RRID:AB_2621445
Rabbit anti-TFEB Antibody	Bethyl Lab.	Cat#A303-673A; RRID:AB_11204751
Chemicals, peptides, and recombinant proteins		
Live/Dead AQUA dead cell stain	Life Technologies	Cat#L34957
Sheep Red Blood Cells	Oxoid	Cat#SR0053B
CD43 (Ly-48) MicroBeads, mouse	Miltenyi Biotec	Cat#130-049-801; RRID:AB_2861373
RPMI-1640 Medium	Sigma-Aldrich	Cat#R8758
HyClone Fetal Bovine Serum	Hyclone	SV30160.03
β-mercaptoethanol	GIBCO	Cat#31350-010

REAGENT or RESOURCE	SOURCE	IDENTIFIER
HEPES	Lonza	Cat#BE17-737E
Penicillin/Streptomycin (5.000 U/ml)	GIBCO	Cat#15070-063
Recombinant Mouse IL-4 Protein	R&D Systems	Cat#404-ML
CellTrace CFSE Cell Proliferation Kit, for flow cytometry	Life Technologies	Cat#C34554
Erythrocyte Lysis Buffer (Buffer EL)	QIAGEN	Cat#79217
Fixation/Permeabilization Solution Kit	BD Biosciences	Cat#554714; RRID:AB_2869008
Click-iT® Plus Edu Alexa Fluor® 647 Flow Cytometry Assay Kit	Life Technologies	Cat#C10634
TRIzol Reagent	Invitrogen	Cat#15596026
RNase-Free DNase Set.	QIAGEN	Cat#79254
SuperScript IV VILO Master Mix	Invitrogen	Cat#11756500
GoTaq® qPCR Master Mix	Promega	Cat#6001
Arcturus PicoPure RNA Isolation kit	Applied Biosystems	Cat#12204-01
CD4 ⁺ T Cell Isolation Kit, mouse	Miltenyi Biotec	Cat#130-104-454
CD45R (B220) MicroBeads, mouse	Miltenyi Biotec	Cat#130-049-501
Collagen, Type I solution	Sigma-Aldrich	Cat#C3867
Dulbecco's MEM (DMEM) F-12 w/o Amino Acids	US Biological Life Science	Cat#D9801-10
Sodium hydrogen carbonate (NaHCO ₃)	Sigma-Aldrich	Cat#1063291000
D-(+)-Glucose solution	Sigma-Aldrich	Cat#G8769
Critical commercial assays		
Mouse IgM ELISA kit	Abcam	Cat#ab133047
Mouse IgG1 ELISA Kit	Abcam	Cat#ab133045
Deposited data		
RNaseq from RagC ^{Q119L/+} GC B cells	This paper	GEO: GSE174003
RNaseq from VavPBcl2/RagC ^{Q119L/+} lymphomas	This paper	GEO: GSE173619
Gene expression profiling in RagC Q119L murine germinal center B cells and B220 ⁺ lymphoma cells	This paper	GEO: GSE174004
Experimental models: Cell lines		
primary B cells	RagC ^{Q119L} mice	N/A
primary T cells	RagC ^{Q119L} mice	N/A
primary MEFs	RagC ^{Q119L} mice	N/A
primary hepatocytes	RagC ^{Q119L} mice	N/A
Experimental models: Organisms/strains		
Rragc ^{Q119L/+}	This Paper	N/A
B6.129S2- <i>Ighm</i> ^{tm1Cgn/J} (Ighm ^{μMT})	The Jackson Laboratory	Cat#002288
VavP-Bcl2	Susanne Cory lab; Walter and Eliza Hall Institute of Medical Research, Melbourne, Victoria, Australia	N/A
Oligonucleotides		
<i>II-6</i> -FW: TACCCCGATTACAGGTGAT.	Ortega-Molina et al., 2015	N/A
<i>II-6</i> -RV: TTGAGCAGAAGAGCTGCTACGT.	Ortega-Molina et al., 2015	N/A

REAGENT or RESOURCE	SOURCE	IDENTIFIER
<i>p21</i> -FW: GTGGGTCTGACTCCAGCCC.	Lopez-Guadamillas et al., 2016	N/A
<i>p21</i> -RV: CCTTCTCGTGAGACGCTTAC	Lopez-Guadamillas et al., 2016	N/A
<i>p16</i> -FW: TACCCCGATTCAAGTGAT.	Lopez-Guadamillas et al., 2016	N/A
<i>p16</i> -RV: TTGAGCAGAAGAGCTGCTACGT	Lopez-Guadamillas et al., 2016	N/A
<i>Il-1b</i> -FW: TCTTTGAAGTTGACGGACCC.	This paper	N/A
<i>Il-1b</i> -RV: TCCACGGGAAAGACACAGGT	This paper	N/A
<i>Ccl2</i> -FW: GGTCCTGTTCATGCTTCTGG	This paper	N/A
<i>Ccl2</i> -RV: GAGTAGCAGCAGGTGAGTGG.	This paper	N/A
<i>Cxcl1</i> -FW: CGCCTATCGCCAATGAGCT.	This paper	N/A
<i>Cxcl1</i> -RV: ATGACTTCGGTTGGGTGCA	This paper	N/A
<i>Cxcl2</i> -FW: GTGAACTGCGCTGTCAATGC.	This paper	N/A
<i>Cxcl2</i> -RV: ACTTCTGTCTGGGCGCAG.	This paper	N/A
<i>Timp1</i> -FW: CTCTGCAACTCGGACCTGG.	This paper	N/A
<i>Timp1</i> -RV: CGCTGGTATAAGGTGGTCTCG	This paper	N/A
<i>Mmp3</i> -FW: GACTCAAGGGTGGATGCTGT.	De Cecco et al., 2019	N/A
<i>Mmp3</i> -RV: CCAACTGCGAAGATCCACTG	De Cecco et al., 2019	N/A
<i>Actin</i> -FW: GGCACCACCTTCTACAATG.	Ortega-Molina et al., 2015	N/A
<i>Actin</i> -RV: GTGGTGGTGAAGCTGTAGCC	Ortega-Molina et al., 2015	N/A
Software and algorithms		
Prism 9 (version 9.1.0)	GraphPad	https://www.graphpad.com
ImageJ	NIH	https://imagej.nih.gov/ij/
FACS DIVA	BD Biosciences	N/A
GSEA software	Subramanian et al., 2005	http://www.gsea-msigdb.org/gsea/index.jsp
Nextpresso pipeline	Graña et al., 2017	http://ubio.bioinfo.cnio.es/people/ograna/nextpresso/ .
TopHat2	Trapnell et al., 2012	https://ccb.jhu.edu/software/tophat/index.shtml
SAMTOOLS v.1.9	Li et al., 2009	http://samtools.sourceforge.net/
Bowtie	Langmead et al., 2009	http://bowtie-bio.sourceforge.net/index.shtml
HTSeq	Anders et al., 2015	https://www-huber.embl.de/HTSeq
DESeq2	Love et al., 2014	http://www.bioconductor.org/packages/release/bioc/html/DESeq2.html .
FlowJo	TreeStar	https://www.flowjo.com
Other		
Flow Cytometry Gating strategy	This paper	Data S1
Uncropped western blots	This paper	Data S2